Nanoscale Mapping of Electrical Resistivity and Connectivity in Graphene Strips and Networks

ARTICLE *in* NANO LETTERS · JANUARY 2011

Impact Factor: 13.59 · DOI: 10.1021/nl101469d · Source: PubMed

5 AUTHORS, INCLUDING:

Pio Peter Niraj Nirmalraj
IBM Research Labs Zurich
23 PUBLICATIONS **3,351** CITATIONS
SEE PROFILE

Shishir Kumar
Indian Institute of Science
24 PUBLICATIONS **359** CITATIONS
SEE PROFILE

Georg S Duesberg
Trinity College Dublin
207 PUBLICATIONS **10,186** CITATIONS
SEE PROFILE

NANO LETTERS

pubs.acs.org/NanoLett

Nanoscale Mapping of Electrical Resistivity and Connectivity in Graphene Strips and Networks

Peter N. Nirmalraj,[†,§] Tarek Lutz,[‡,§] Shishir Kumar,[†,§] Georg S. Duesberg,[†,§] and John J. Boland*[,†,§]

[†]School of Chemistry, [‡]School of Physics, and [§]Center for Research on Adaptive Nanostructures and Nanodevices (CRANN), Trinity College Dublin, Dublin 2, Ireland

ABSTRACT In this article we map out the thickness dependence of the resistivity of individual graphene strips, from single layer graphene through to the formation of graphitic structures. We report exceptionally low resistivity values for single strips and demonstrate that the resistivity distribution for single strips is anomalously narrow when compared to bi- and trilayer graphene, consistent with the unique electronic properties of single graphene layers. In agreement with theoretical predictions, we show that the transition to bulklike resistivities occurs at seven to eight layers of graphene. Moreover, we demonstrate that the contact resistance between graphene flakes in a graphene network scales with the flake thickness and the implications for transparent conductor applications are discussed.

KEYWORDS Graphene resistivity, interflake resistance, conductance imaging atomic force microscopy (CI-AFM);

Ever since the pioneering observations of Novoselov et al,[1] graphene has continued to attract widespread research interest. As a single layer material, graphene has interesting electronic properties such as ballistic transport,[2] a quantum Hall effect at room temperature,[3,4] and a size-dependent band gap,[5,6] all of which may enable new kinds of nanoscale electronic devices and sensors. Improvement in the mechanical[7] and solvent-based processing and synthesis of graphene,[8] combined with the ability to transfer these materials from one substrate to another[9,10] have now opened the door to other possible applications. For instance, graphene's excellent in-plane conductivity and the ability to make ultrathin materials with limited optical absorption are particularly suited to transparent and flexible electronics applications.[11,12] Before these applications can be realized, however, a thorough understanding of transport in graphene films is required. Even at this early stage significant experimental and theoretical studies have already been conducted, as detailed in the recent review by Castro et al.[5] However, most experimental studies performed to date have relied on conventional bulk electrical characterization methods to probe the electronic behavior of monolayer and bilayer graphene[3,6,13−18] which are not amenable to studies of transport over different length scales or investigations of the roles of intrinsic or patterned defects. Additionally, it is not well understood how individual monolayer or multilayer flakes interact and make contact with each other within a graphene film and how to optimize these interactions for any particular application. Here we study the nanoscale electronic properties of graphene strips of varying thicknesses. We demonstrate how the resistivity of individual graphene strips scale as their thickness is increased from a single monolayer to larger thicknesses using local nanoscale probe measurements and how the resistivity values ultimately approach that of bulk graphite. Moreover, we measure the resistance drop between flakes in graphene film networks and show how it scales with the thickness of interconnecting flakes and discuss the implications for the use of graphene films in transparent conductor applications.

The graphene films used in this study were synthesized using a chemical vapor deposition technique that was recently shown as a potential route to large scale graphene film growth.[12,19] We chose this approach over mechanical exfoliation[1] used previously to investigate few layer graphene (FLG) or liquid phase exfoliation of graphite[8] in organic solvents, which typically leads to smaller sized flakes. In order to investigate single graphene flakes we subjected the initial grown films to a peeling process using Scotch tape that also allowed us to investigate films of varying thicknesses. Graphene films were grown in a hot-wall chemical vapor deposition (CVD) furnace on a nickel catalyst surface.[19] After the underlying nickel was etched with hydrochloric acid, subsequently the films were transferred onto SiO_2 substrates (300 nm of thermally grown oxide). Palladium electrodes (25 nm) were sputtered onto the graphene films after electron beam lithography. The samples were annealed in an atmosphere of Ar/H_2 for 2 h at 400 °C to remove any photoresist residues remaining from the lithographic process[20] and to ensure reliable contacts. All electrical measurements were

* Corresponding author: phone number, +3531896 3140; fax number, +3531896 3142; e-mail address, jboland@tcd.ie.

Received for review: 04/26/2010
Published on Web: 12/03/2010

DOI: 10.1021/nl101469d | *Nano Lett.* **2011,** *11,* 16–22

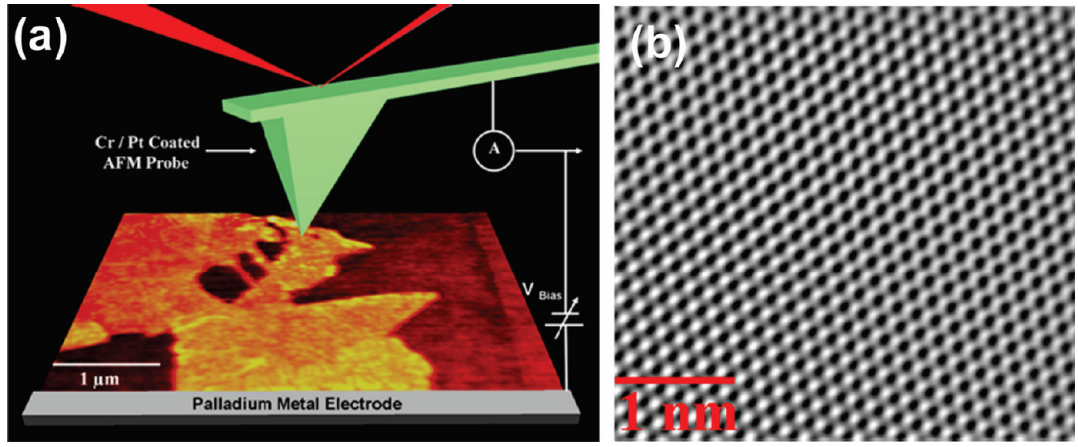

FIGURE 1. (a) Schematics for the CI-AFM technique showing the local probe measurement setup on monolayer graphene flakes. (b) TEM imaging of the atomic structure of graphene revealing the hexagonal arrangement of the planar carbon atoms.

performed using conductance imaging atomic force microscopy (CI-AFM). This technique has been employed previously to probe the local electronic properties of carbon nanotubes,[21−23] to optimize the contact resistance between carbon nanotubes and metal electrodes,[24] and to measure the conductivity of DNA molecules.[25] The CI-AFM technique was implemented using the conducting probe as a mobile contact which was held at ground potential and made to scan over the material of interest that is electrically connected to the biased Pd electrode (see Figure 1a schematic). The probe used in the CI-AFM technique is coated with Pt/Cr conductive coating (Cont E, resonant frequency 13 kHz, force constant 0.2 N/m). All CI-AFM measurements were performed under an optimum loading force of ∼1 nN. The contact resistance between the metal probe and the metal electrode was ∼250 Ω in the case of Pd and ∼580 Ω in the case of Ti/Au, and this was checked repeatedly during measurements to verify the cleanliness and the electrical performance of the tip. This contact resistance associated with the external circuit between the probe and the electrode was subtracted in all the presented data so that the intercepts and slopes of the data presented correspond to the combined electrode−graphene and probe−graphene contact resistance and the linear graphene resistance, respectively (see below).

Figure 1a is a schematic showing the CI-AFM setup. Measurements were performed on pristine as-grown graphene films transferred to a SiO_2 substrate. The thickness distribution of the transferred graphene films was determined using AFM in tapping mode. The average thicknesses of graphene flakes found within the as-grown film and a film subjected to repeated peeling process are 6.5 ± 0.35 and 3.5 ± 0.25 nm (see Supporting Information), respectively. The average thickness of a single graphene flake relative to the SiO_2 substrate (300 nm oxide thickness) obtained from our atomic force microscopy (AFM) analysis is 0.6 ± 0.2 nm (see Supporting Information). Previous studies have estimated the thickness of a single graphene flake to vary from 0.35 to 1.6 nm.[1,13,16,17] In contrast, STM measurements in ultrahigh vacuum conditions have reported monolayer graphene thickness of 0.42 nm,[20] consistent with 0.34 nm height which is the interlayer spacing in bulk graphite. The larger reported AFM values are due to the presence of adsorbed oxygen during ambient measurements. Figure 1b is a high-resolution TEM image of one of our graphene samples and demonstrates that the materials used in this study are of excellent quality.

Panels a and b of Figure 2 are topographic and current maps of a thick graphene film that was transferred to a SiO_2 substrate. The film is electrically homogeneous as indicated by the near constant current values measured at different points in the film. The topography also complements the current map data by showing well interconnected flakes of graphene with wrinkles appearing in certain regions. Figure 2c shows a 3D rendering of the outlined area in Figure 2a where the formation of wrinkles is clearly evident. The average height of the wrinkles is ∼4 nm relative to the surface, and the tip also records a higher current value in these wrinkled regions. The wrinkles are formed primarily during the cooling phase in the growth process as nickel contracts more than graphene due to its larger thermal expansion coefficient. In addition to thermal stress it has been shown that the nucleation of defect lines on step edges between Ni terraces leads to the formation of wrinkles.[26] CI-AFM measurements were also performed on graphene samples that were subjected to repeated peeling (∼10 times) and rinsing in acetone followed by blow drying in nitrogen gas. Afterward CI-AFM showed a very sparse film: the topography (Figure 2d) and the corresponding current map (Figure 2e) show the current to vary from one region to another as certain regions were observed to be more resistive than others, and in some areas the SiO_2 substrate is exposed. Figure 2f is a magnified section of the current map (area marked in red square in Figure 2e), where there are significant local variations in the film conductivity.

DOI: 10.1021/nl101469d | *Nano Lett.* **2011,** *11,* 16–22

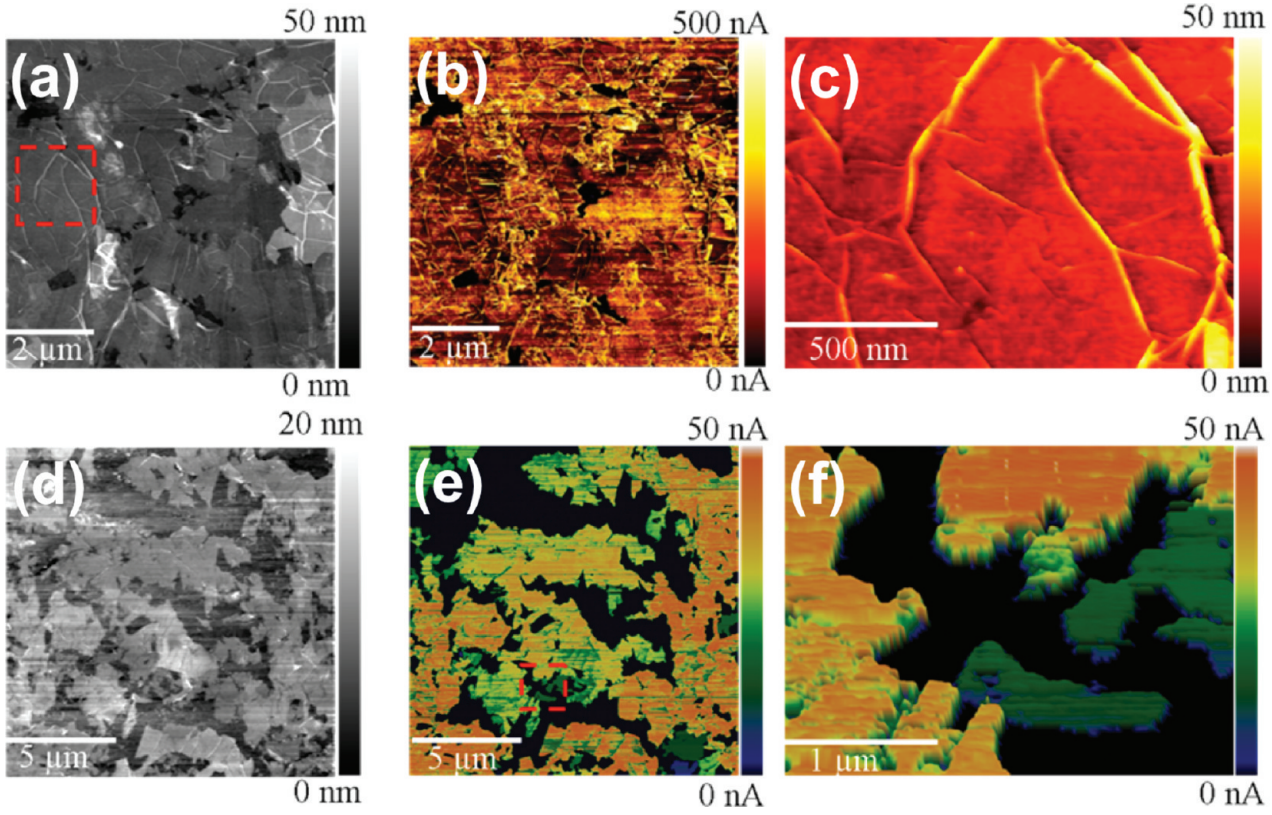

FIGURE 2. CI-AFM results for thick and sparse graphene films. (a, b) Topography and current map of thick graphene film showing the uniformity in electrical conductance across the film. The graphene flakes are well interconnected within the film leading to high conductance even when 100 μm away from the electrode. (c) A 3D view of the topography of the wrinkles from a selected region (marked in red square) of panel a (scanning conditions: V_{bias}, 1 mV; preamplifier sensitivity, 100 nA/V). (d, e) Topography and current map of a sparse graphene film showing local electronic variations within the graphene flakes. The electrode is at the right-hand side of the image. The local electronic discrepancy is well highlighted in the 3D image shown in part f, which is from the highlighted area in panel e (scanning conditions: V_{bias}, 2 mV, preamplifier sensitivity, 100 nA/V).

Local variations in the conductivity of sparse films (Figure 2e) have important implications for performance of transparent conductors and can be analyzed with the aid of high-resolution current maps that detail transport within and between flakes. The electrical resistivity within a single flake can be determined using the CI-AFM technique; however, for two-dimensional systems like graphene the current spreads laterally. In order to extract the resistivity of the graphene the as synthesized CVD grown graphene flakes were patterned and etched using standard optical lithographic process to produce graphene strips with well-defined lengths and widths (see Supporting Information). In all cases the patterned strips were sufficiently large so as to suppress quantum size effects. The structured graphene strips contacted by metal electrodes were then analyzed using the CI-AFM technique with a highly sensitive preamplifier (TUNA module, Veeco systems) as shown in Figure 3a and the local variations in the measured resistance are plotted as a function of the distance (x) from the electrode (blue plot in Figure 3b) where the resistance shown at each distance value x is an average of that recorded at ~10 locations across the width of the graphene strip as shown in the plot in Figure 3b. The resistance measured across the width of the graphene strip shows the edges to be less resistive when compared to the center of the strip as seen from the current map (see Supporting Information) and the resistance trace plots, and most likely due to enhanced contact between the edge and probe. The measured resistance (R) can be expressed as

$$R(x) = R_{\text{Contact}} + R_{\text{Graphene}(l,w,t)} = R_{\text{Contact}} + \rho x/(wt)$$

where $R_{\text{Graphene}(l,w,t)}$ is the resistance of a graphene strip (length l, width w, thickness t) and R_{Contact} is the combined contact resistance due to the probe−graphene, graphene−electrode contacts and the spreading resistance associated with point probe contact method used in these measurements. To ensure that the contact contributions remain constant, a fixed loading force (1 nN) was used in all experiments and the possible degradation of the metal coated probe was tested by routinely by measuring the resistance between the probe and the contacting electrode. When the loading force was increased while scanning in contact mode from 1 to 3.5 nN, the contact resistance is decreased by a few ohms but the slope of the resistance versus distance curve does not undergo any significant

DOI: 10.1021/nl101469d | *Nano Lett.* **2011,** *11,* 16–22

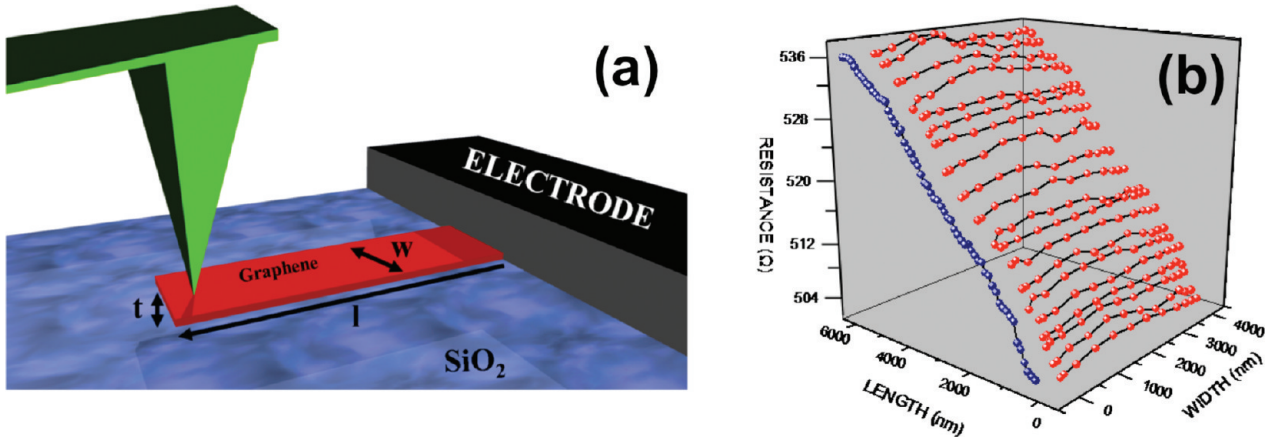

FIGURE 3. Resistivity calculations for graphene strips. (a) Schematic for resistivity measurements on structured graphene strips with well-defined dimensions. (b) Plot of the local resistance variations across the graphene flake as a function of distance from the electrode (blue trace). The resistance is observed to increase gradually as the tip measures away from the electrode. Furthermore these data are obtained by measuring the resistance across the width of the graphene strip and by taking the average resistance value from ~10 data points across the strip as shown in the 3D plot in part b.

change (see Supporting Information). The graphene resistivity (ρ) can be calculated from eq 1 below

$$\rho = (dR/dx)wt \quad (1)$$

Using this equation we can estimate the resistivity of a graphene strip from the slope (blue trace) in Figure 3b and the known dimensions (thickness, 0.45 nm; width, 4.2 μm; length, 5.8 μm, see Supporting Information) to be $\sim 0.01 \times 10^{-6}$ Ω m. Similar measurments performed on over 20 monolayer graphene strips yield a mean single strip resistivity of 0.03×10^{-6} Ω m. This resistivity value is comparable but higher than the reported value of 0.01×10^{-6} Ω m by Chen et al[27] for monolayer graphene. However, it is important to note that the resistivity measurements may be influenced by the underlying SiO_2 substrate which is known to limit the intrinsic electronic properties of monolayer graphene through the presence of trapped charges,[28,29] interfacial phonons,[27] substrate induced structural distortions,[20,30] or other external impurities as all CI-AFM measurements were performed under ambient conditions.[31]

We repeated the resistivity measurements for graphene strips of different thicknesses, and the data are shown in Figure 4. The relative noise in the data is striking, showing the smallest values for single layer graphene. These data point to the uniqueness of single layer graphene which has an exceptionally narrow resistivity distribution that is fundamentally different from few layer graphene (FLG), where the possibility of different stacking sequences and absorbate intercalation yields dramatically wider distributions. The transition in the electronic behavior of graphene to graphite has been previously predicted by first principles calculations[32] to occur at thicknesses of approximately eight monolayers. This agrees well with the data in Figure 4 where a knee in the resistivity curve (blue arrow in Figure 4) is

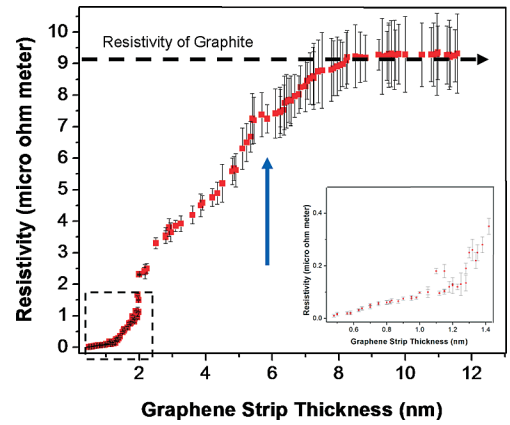

FIGURE 4. Measurement of resistivity as a function of the strip thickness. A clear trend is observed where the resistivity increases upon increasing the number of layers in a graphene strip. The distinct knee (indicated by blue arrow) in the curve is observed at a thickness of 5−6 nm, which corresponds to seven to eight monolayers, highlights the transistion in the electronic behavior of graphene to graphite. At the largest thickness studied (10−12 nm) the resistivity approaches 9×10^{-6} Ω m, which is in good agreement with the known resistivity of graphite.

observed at a thickness of 5−6 nm, which corresponds to seven to eight monolayers. At the largest thickness studied (10−12 nm) the resistivity approaches 9×10^{-6} Ω m, which is in good agreement with the known resistivity of graphite.[33] Although the thickness evolution in graphene films has been investigated using angle-resolved photoemission spectroscopy[34] this is the first detailed experimental study reported on the thickness dependence of the resistivities of individual graphene strips.

CI-AFM can also investigate the resistance between flakes within a graphene film. Figure 5a shows a typical current map between a monolayer layer flake (flake 1, thickness ~0.8 nm) and a bilayer flake (flake 2, thickness ~1.1 nm). Flake 1 is connected to the electrode (not shown), and as the resistance is traced along this flake, we observe a value

DOI: 10.1021/nl101469d | *Nano Lett.* **2011,** *11,* 16–22

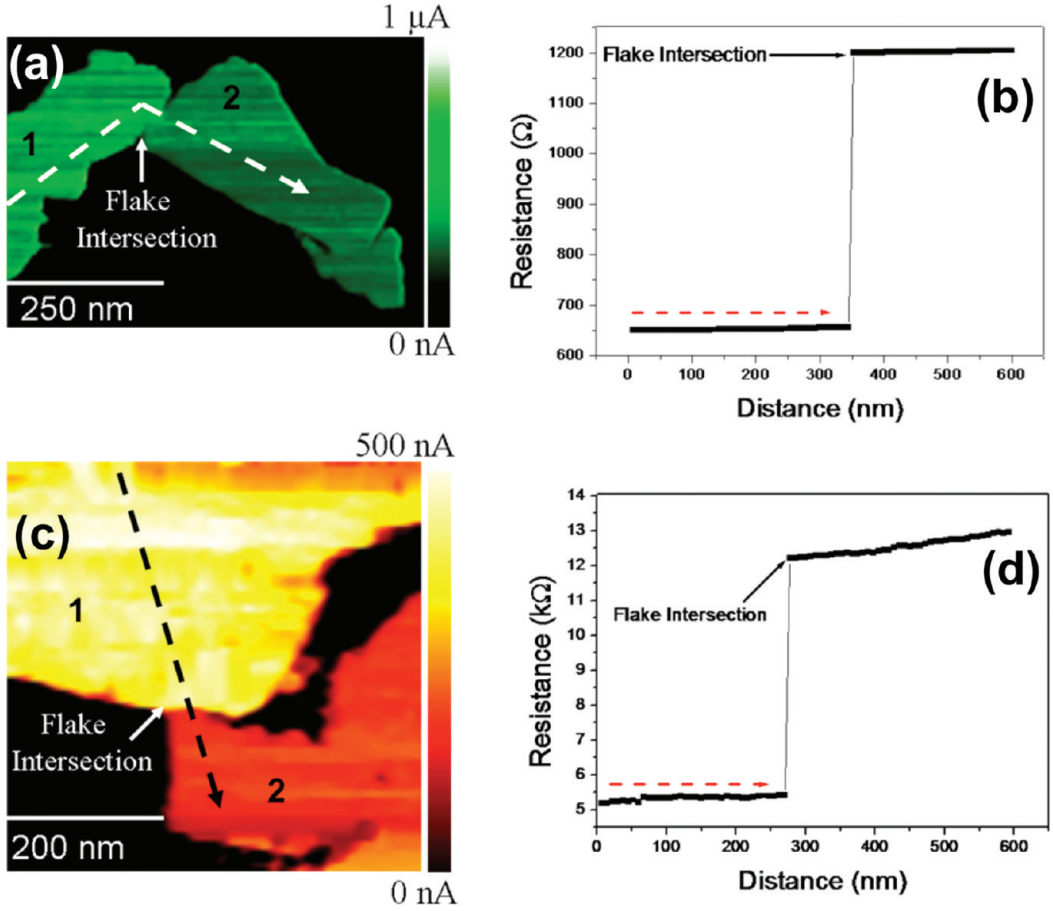

FIGURE 5. Interflake resistance analysis between graphene flakes of varying thicknesses. (a) Current map of a monolayer graphene flake (flake 1) connected to the electrode on the left-hand side of the image (not shown) and is interconnected to a bilayer graphene flake (flake 2). There is a clear difference in the current measured within flake 1 and flake 2 seen from the color coding of the current map. (b) Tracing the resistance along flake 1 and as the tip scans across flake 2, a jump in the local resistance is measured at the intersection between the two flakes. This measured interflake resistance is ~550 Ω; continuing the trace shows the resistance to be stable across flake 2. (c) Current map of a multilayer graphene flake (flake 1) contacting a trilayer graphene flake (flake 2) at an intersection point. Flake 1 is connected to the electrode on top of the image (not shown). There is a huge increase in resistance at the junction between the two flakes of ~6.5 kΩ as shown in section d, where the local resistance is traced as a function of distance from the electrode. The dashed red arrows in sections b and d indicate the direction along which the resistance is traced (scanning conditions: V_{bias}, 0.4 mV (a); V_{bias}, 1.5 mV; (c) preamplifier sensitivity, 100 nA/V).

of ~650 Ω with small fluctuations. Proceeding onto flake 2 there is a clear increase in the measured resistance at the intersection between the two flakes as is clearly shown by the local resistance versus distance curve in Figure 5b. The interflake resistance jump is ~550 Ω at the intersection between flakes and remains approximately constant as the trace continues along flake 2. Similar measurements have been performed on a large number of adjoining flakes, and in each case the measured resistance jump was found to be dependent on the thickness of the flakes that comprise the junction. Figure 5c shows a current map of a junction formed between a multilayer flake (thickness ~5 nm) and a trilayer flake (thickness ~2.2 nm). The presence of a large voltage drop at the intersection between the flakes is immediately evident in the current map (Figure 5c) and the corresponding resistance jump of 6.5 Kohm (Figure 5d) show a corresponding resistance jump of ~6.5 kΩ. Beyond the overlap region the resistance is once again found to be slowly increasing reflecting the increased resistivity of the thicker flake, Analysis of approximately ~100 interflake contacts shows the interflake resistance to be highly dependent on the thicknesses of the upper flake, with the lowest resistance occurring between individual graphene flakes and the highest values associated with junctions comprised of thicker flakes.

Figure 6 shows a plot of the interflake resistance as a function of the thickness of the upper flake (see schematic inset). This linear dependence of the interflake resistance on the thickness of the top flake has not been reported before and has important implications for large area graphene films. One reason for this behavior is that interflake connectivity necessitates charge transport perpendicular to the graphene sheets in the top flake and so the resistance scales with the number of such sheets. The observed scatter is also

DOI: 10.1021/nl101469d | *Nano Lett.* **2011,** *11,* 16–22

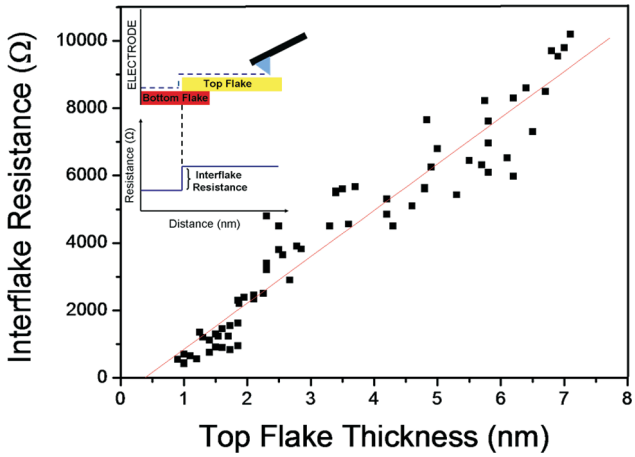

FIGURE 6. Analysis of interflake resistance as a function of the top flake thickness. The measured interflake resistance is found to increase as the thickness of the top flake increases. These data are mainly based on the contacts between two flakes where one flake overlaps the other. The thickness distribution of the flakes analyzed for this measurement ranges from 1 to 7.5 nm.

significant. While some level of scatter may be attributable to variations in the flake overlap area, previous studies by Castro et al.[5] and Novoselov et al.[1] have highlighted that stacking in bilayer and few layer graphene dominates charge transport and that increasing the number of graphene layers changes the local electronic behavior of these systems. Thus the stacking sequence in thicker graphene flakes may depart from the expected ordered ABAB stacking which will modify the electronic coupling through the flake. In addition we note that measurements with single-layer contacts are challenging since their occurrence is quite rare following our peeling preparation. However, by extrapolating the flake thickness data in Figure 6 to the theoretically feasible graphene flake thickness of ~0.35 nm, it should then be possible to attain very low interflake resistance values (less than 100 Ω) between the overlapping flakes. Such low interflake resistance values should be compared to 100 kΩ in the case of contacts between individual single-walled carbon nanotubes[24] such that graphene networks should have superior electrical performance for flexible electronics and displays applications.

In summary, we have mapped out the thickness dependence of the resistivity of individual graphene strips starting from single layers all the way through to the formation of graphitic structures. We report on the CI-AFM measured resistivity values for single graphene strips and demonstrate that the resistivity distribution for single strips is anomalously narrow compared to even bi- and trilayer graphene and consistent with the unique electronic properties of single layer graphene. In agreement with theoretical predictions, we show that the transition to bulklike resistivities occurs at seven to eight monolayer thick strips and that the resistance between flakes scales with flake thickness. These results demonstrate that optimally transparent and conducting graphene films can be formed by single layer graphene with minimal overlap between flakes.

Acknowledgment. We acknowledge the Science Foundation Ireland funded collaboration (SFI Grant 03/CE3/M406s1) between Trinity College Dublin, University College Cork, and Hewlett-Packard, Dublin Inkjet Manufacturing Operation, and the SFI Principal Investigator (Grant No. 06/IN.1/I106) and CSET award which facilitated this work to take place. We would also like to thank INSPIRE for supporting our work in the advanced microscopy laboratory and Dr Valeria Nicolosi (Oxford University) for HRTEM work. We also acknowledge the Embark Initiative for IRCEST scholarships for Shishir Kumar.

Supporting Information Available. Statistical information for the thickness of the graphene flakes within the network, synthesis procedure and current map of the graphene strips have been provided. The analysis of contact resistance as a function of loading force between the metal probe and the graphene strip. This material is available free of charge via the Internet at http://pubs.acs.org.

REFERENCES AND NOTES

(1) Novoselov, K. S.; Geim, A. K.; Morozov, S. V.; Jiang, D.; Zhang, Y.; Dubonos, S. V.; Grigorieva, I. V.; Firsov, A. A. *Science* **2004**, *306*, 666–669.
(2) Miao, F.; Wijeratne, S.; Zhang, Y.; Coskun, U. C.; Bao, W.; Lau, C. N. *Science* **2007**, *317*, 1530–1533.
(3) Abanin, D. A.; Novoselov, K. S.; Zeitler, U.; Lee, P. A.; Geim, A. K.; Levitov, L. S. *Phys. Rev. Lett.* **2007**, *98*, 196806.
(4) Novoselov, K. S.; Jiang, Z.; Zhang, Y.; Morozov, S. V.; Stormer, H. L.; Zeitler, U.; Maan, J. C.; Boebinger, G. S.; Kim, P.; Geim, A. K. *Science* **2007**, *315*, 1379.
(5) Castro Neto, A. H.; Guinea, F.; Peres, N. M. R.; Novoselov, K. S.; Geim, A. K. *Rev. Mod. Phys.* **2009**, *81*, 109–162.
(6) Nilsson, J.; Neto, A. H.; Guinea, F.; Peres, N. M. *Phys. Rev. Lett.* **2006**, *97*, 266801.
(7) Lee, C.; Wei, X.; Kysar, J. W.; Hone, J. *Science* **2008**, *321*, 385–388.
(8) Hernandez, Y.; Nicolosi, V.; Lotya, M.; Blighe, F. M.; Sun, Z.; De, S.; McGovern, I. T.; Holland, B.; Byrne, M.; Gun'Ko, Y. K.; Boland, J. J.; Niraj, P.; Duesberg, G.; Krishnamurthy, S.; Goodhue, R.; Hutchison, J.; Scardaci, V.; Ferrari, A. C.; Coleman, J. N. *Nat. Nanotechnol.* **2008**, *3*, 563–568.
(9) Li, X.; Zhu, Y.; Cai, W.; Borysiak, M.; Han, B.; Chen, D.; Piner, R. D.; Colombo, L.; Ruoff, R. S. *Nano Lett.* **2009**, *9*, 4359–4363.
(10) Reina, A.; Jia, X.; Ho, J.; Nezich, D.; Son, H.; Bulovic, V.; Dresselhaus, M. S.; Kong, J. *Nano Lett.* **2008**, *9*, 30–35.
(11) Cai, W.; Zhu, Y.; Li, X.; Piner, R. D.; Ruoff, R. S. *Appl. Phys. Lett.* **2009**, *95*, 123115–123113.
(12) Kim, K. S.; Zhao, Y.; Jang, H.; Lee, S. Y.; Kim, J. M.; Kim, K. S.; Ahn, J. H.; Kim, P.; Choi, J. Y.; Hong, B. H. *Nature* **2009**, *457*, 706–710.
(13) Casiraghi, C.; Hartschuh, A. L.; Qian, E.; Harutyunyan, H.; Gokus, T.; Novoselov, K. S.; Ferrari, A. C. *Nano Lett.* **2007**, *7*, 2711–2717.
(14) Casiraghi, C.; Hartschuh, A.; Qian, H.; Piscanec, S.; Georgi, C.; Fasoli, A.; Novoselov, K. S.; Basko, D. M.; Ferrari, A. C. *Nano Lett.* **2009**, *9*, 1433–1441.
(15) Castro, E. V.; Novoselov, K. S.; Morozov, S. V.; Peres, N. M.; dos Santos, J. M.; Nilsson, J.; Guinea, F.; Geim, A. K.; Neto, A. H. *Phys. Rev. Lett.* **2007**, *99*, 216802.
(16) Chen, Z.; Lin, Y. M.; Rooks, M. J.; Avouris, P.; Physica, E. *Phys. E (Amsterdam, Neth.)* **2007**, *40*, 228–232.
(17) Gupta, A.; Chen, G.; Joshi, P.; Tadigadapa, S.; Eklund, *Nano Lett.* **2006**, *6*, 2667–2673.
(18) Kuzmenko, A. B.; Benfatto, L.; Cappelluti, E.; Crassee, I.; van der Marel, D.; Blake, P.; Novoselov, K. S.; Geim, A. K. *Phys. Rev. Lett.* **2009**, *103*, 116804.

DOI: 10.1021/nl101469d | *Nano Lett.* **2011,** *11,* 16–22

(19) Kumar, S.; McEvoy, N.; Lutz, T.; Keeley, G. P.; Nicolosi, V.; Murray, C. P.; Blau, W. J.; Duesberg, G. S. *Chem. Commun. (Cambridge, U.K.)* , *46*, 1422–1424.
(20) Ishigami, M.; Chen, J. H.; Cullen, W. G.; Fuhrer, M. S.; Williams, E. D. *Nano Lett.* **2007**, *7*, 1643–1648.
(21) de Pablo, P. J.; Martinez, M. T.; Colchero, J.; Gomez-Herrero, J.; Maser, W. K.; Benito, A. M.; Munoz, E.; Baro, A. M. *Adv. Mater.* **2000**, *12*, 573–576.
(22) Fujiwara, A.; Iijima, R.; Suematsu, H.; Kataura, H.; Maniwa, Y.; Suzuki, S.; Achiba, Y. *Phys. B (Amsterdam, Neth.)* **2002**, *323*, 227–229.
(23) Nirmalraj, P. N.; Lyons, P. E.; De, S.; Coleman, J. N.; Boland, J. J. *Nano Lett.* **2009**, *9*, 3890–3895.
(24) Nirmalraj, P. N.; Boland, J. J. *ACS Nano* **2010**, *4*, 3801–3806.
(25) Heim, T.; Deresmes, D.; Vuillaume, D. *J. Appl. Phys.* **2004**, *96*, 2927–2936.
(26) Chae, S. J.; et al. In Carbon Nanotubes, Graphene, and Associated Devices, II.1 ed; SPIE: Bellingham, WA, 2009; 73990W-73911.
(27) Chen, J.-H.; Jang, C.; Xiao, S.; Ishigami, M.; Fuhrer, M. S. *Nat. Nanotechnol.* **2008**, *3*, 206–209.
(28) Chen, J. H.; Jang, C.; Adam, S.; Fuhrer, M. S.; Williams, E. D.; Ishigami, M. *Nat. Phys.* **2008**, *4*, 377–381.
(29) Nomura, K.; MacDonald, A. H. Q. *Phys. Rev. Lett.* **2006**, *96*, 256602.
(30) Morozov, S. V.; Novoselov, K. S.; Katsnelson, M. I.; Schedin, F.; Elias, D. C.; Jaszczak, J. A.; Geim, A. K. *Phys. Rev. Lett.* **2008**, *100*, No. 016602.
(31) Schedin, F.; Geim, A. K.; Morozov, S. V.; Hill, E. W.; Blake, P.; Katsnelson, M. I.; Novoselov, K. S. *Nat. Mater.* **2007**, *6*, 652–655.
(32) AlZahrani, A. Z.; Srivastava, G. P. *J. Phys.: Conden. Matter* **2009**, *21*, 495503.
(33) Powell, R. L.; Childs, G. E. In *American Institute of Physics Handbook*; AIP: New York, 1972; pp 140−160.
(34) Ohta, T.; Bostwick, A.; McChesney, J. L.; Seyller, T.; Horn, K.; Rotenberg, E. *Phys. Rev. Lett.* **2007**, *98*, 206802.

DOI: 10.1021/nl101469d | *Nano Lett.* **2011,** *11,* 16–-22